



**HAL**  
open science

## **DNAPL accumulation in wells and DNAPL recovery from wells: model development and application to a laboratory study**

Brent E. Sleep, Sandra Beranger, Stefan Reinecke, Yves Filion

► **To cite this version:**

Brent E. Sleep, Sandra Beranger, Stefan Reinecke, Yves Filion. DNAPL accumulation in wells and DNAPL recovery from wells: model development and application to a laboratory study. *Advances in Water Resources*, 2015, 85, pp.109-119. 10.1016/j.advwatres.2015.09.023 . hal-01307784

**HAL Id: hal-01307784**

**<https://brgm.hal.science/hal-01307784>**

Submitted on 22 Jun 2022

**HAL** is a multi-disciplinary open access archive for the deposit and dissemination of scientific research documents, whether they are published or not. The documents may come from teaching and research institutions in France or abroad, or from public or private research centers.

L'archive ouverte pluridisciplinaire **HAL**, est destinée au dépôt et à la diffusion de documents scientifiques de niveau recherche, publiés ou non, émanant des établissements d'enseignement et de recherche français ou étrangers, des laboratoires publics ou privés.

1 **DNAPL Accumulation in Wells and DNAPL Recovery from Wells: Model**  
2 **Development and Application to a Laboratory Study**

3  
4 Brent E. Sleep<sup>a\*</sup>, Sandra Beranger<sup>b</sup>, Stefan Reinecke<sup>c</sup>, Yves Filion<sup>d</sup>

5 <sup>a</sup> Department of Civil Engineering, University of Toronto, Toronto, Canada

6 <sup>b</sup> Bureau de Recherches Géologiques et Minières, Toulouse, France

7 <sup>c</sup> Stratos, Ottawa, Canada

8 <sup>d</sup> Department of Civil and Environmental Engineering, Queen's University, Kingston,  
9 Canada

10 \* Corresponding Author

11  
12 **ABSTRACT**

13 Dense nonaqueous phase liquid (DNAPL) accumulation and recovery from wells cannot  
14 be accurately modeled through typical pressure or flux boundary conditions due to  
15 gravity segregation of water and DNAPL in the wellbore, the effects of wellbore storage,  
16 and variations of wellbore inflow and outflow rates with depth, particularly in  
17 heterogeneous formations. A discrete wellbore formulation is presented for numerical  
18 modeling of DNAPL accumulation in observation wells and DNAPL removal from  
19 recovery wells. The formulation includes fluid segregation, changing water and DNAPL  
20 levels in the well and the corresponding changes in fluid storage in the wellbore. The  
21 method was added to a three-dimensional finite difference model (CompSim) for three  
22 phase (water, gas, DNAPL) flow. The model predictions are compared to three-  
23 dimensional pilot scale experiments of DNAPL (benzyl alcohol) infiltration,  
24 redistribution, recovery, and water flushing. Model predictions match experimental  
25 results well, indicating the appropriateness of the model formulation. Characterization of  
26 mixing in the extraction well is important for predicting removal for highly soluble  
27 organic compounds like benzyl alcohol. A sensitivity analysis shows that the  
28 incorporation of hysteresis is critical to accurate prediction. Among the multiphase flow  
29 and transport parameters required for modelling, results are most sensitive to soil intrinsic  
30 permeability.

1 **1. INTRODUCTION**

2  
3 Remediation of groundwater contamination from the presence of dense nonaqueous  
4 phase liquids (DNAPL) remains a challenge. The discovery of DNAPLs in the  
5 subsurface, and inferences about amounts of DNAPLs present in soils are often related to  
6 observations of DNAPL accumulation in wells. Some degree of DNAPL recovery from  
7 the subsurface may be achieved through water flooding (Gerhard et al., 1998; Alexandra  
8 et al., 2012), or by single or dual phase extraction (Gerhard et al., 2001). For field-scale  
9 application of these methods models that can accurately simulate the dynamics of  
10 multiphase fluid flow between wells and soil could be very useful design tools.

11  
12 Sleep et al. (2000a) presented a method for modeling light nonaqueous phase liquids  
13 (LNAPL) accumulation in wells. The most significant feature of the model compared to  
14 other multiphase models with special treatment of wells (Behie et al., 1985; Collins et al.,  
15 1992; Lacombe et al., 1995; Forsyth and Sudicky, 1998; Wu, 2000) was the inclusion of  
16 gravity segregation of fluids in a wellbore that is connected to several gridblocks in a  
17 finite difference grid. When gravity segregation occurs in a well in a system containing  
18 DNAPL, DNAPL entering the well will accumulate at the bottom of the well, and water  
19 will pool on top of the DNAPL. Air will accumulate at the top of the well. When fluid  
20 flow occurs from the well to the soil the flow of a particular phase can only occur from  
21 the sections of the wellbore containing that particular phase. When flow of a particular  
22 fluid is from the soil into the well, the fluid can only flow into the well from grid blocks  
23 that are at pressures greater than the pressure in the adjacent wellbore section. For  
24 example, in the case of grid blocks connected to the air-filled section of the wellbore,  
25 water or DNAPL from these blocks can only flow into the well if the grid block water or  
26 DNAPL pressure is greater than the air pressure in the wellbore (similar to a seepage  
27 face).

28  
29 In the current study a model is developed for simulation of DNAPL accumulation in  
30 wells and DNAPL recovery from wells. The wellbore formulation accounts for the  
31 accumulation of DNAPL at the bottom of the wellbore. Corresponding relationships are

1 incorporated into the model for calculation of pressures and relative permeabilities for  
2 each phase present in the wellbore at any time. The model is applied to pilot scale tests of  
3 benzyl alcohol (BA) infiltration and recovery. Predicted BA and water levels in wells and  
4 BA recovery rates are compared to measured values to test the model and a sensitivity  
5 analysis is performed to determine the sensitivity of the model to various soil and fluid  
6 parameters.

7

## 8 **2. MODELING DISCRETE WELLBORE DYNAMICS WITH FLUID** 9 **STRATIFICATION**

10 To simulate wells in finite difference multiphase flow models, it is assumed that head  
11 drops along the wellbore are insignificant and that each well can be represented by one  
12 finite difference cell divided into sections that are aligned with the vertical grid divisions  
13 surrounding the wellbore (Figure 1). The wellbore cell is connected to several regular soil  
14 gridblocks. For this wellbore cell, the fluid saturations and fluid pressures must be known  
15 at each time step of a simulation. In practice, recovery wells are usually constructed with  
16 a relatively homogeneous sand pack along the well screen and a sump at the bottom of  
17 the well to prevent DNAPL from flowing out the bottom of the well. The sand packs  
18 typically would have different properties than the surrounding soils and may be a  
19 preferential path for vertical DNAPL migration. To simulate the presence of a sandpack  
20 the soil gridblocks containing the wellbore cell may have properties assigned to represent  
21 the sandpack properties, although as a finite difference grid is used, the soil gridblocks  
22 would be rectangular and not precisely simulate the geometry of an annular sand pack.  
23 The sump can be simulated by extending the bottom of the wellbore into soil gridblocks  
24 below the screen location but not allowing any connection (i.e. zero transmissivity  
25 between wellbore and soil gridblock) between the wellbore and these soil gridblocks  
26 adjacent to the sump portion of the wellbore.

27

28 To model fluid flow between the well sections and soil gridblocks it is necessary to  
29 calculate the location of the air-water and water-DNAPL interfaces with time. From the  
30 overall water, air, and DNAPL saturations in the well cell the location of the fluid  
31 interfaces can be calculated from the wellbore length and elevation of the bottom of the

1 wellbore. If the wellbore fluids are in mechanical equilibrium, and the position of the  
2 interfaces and phase densities are known, the pressure at any elevation in the well can be  
3 calculated from the thicknesses of air, water, and DNAPL above that elevation, the fluid  
4 densities, and the gas pressure at the top of the wellbore.

5  
6 With the pressure in the wellbore section calculated at the elevation of the gridblock  
7 centre, the flow of each of the three phases between the wellbore section and the  
8 gridblock can be calculated from the pressure difference between the wellbore and the  
9 gridblock, and the phase transmissivity for wellbore-gridblock flow. The transmissivities  
10 will depend on wellbore block length and diameter in the gridblock in question, soil  
11 permeabilities, and phase relative permeabilities in the wellbore and the gridblock soil.  
12 The equation for wellbore-gridblock flow is given by:

$$13 \quad q_{\beta} = T_{\beta} (h_{\beta} - h_{\beta}^w) \quad (1)$$

14 where  $\beta$  represents the phase (water, air, or DNAPL),  $q_{\beta}$  is the wellbore-gridblock Darcy  
15 flow rate,  $h_{\beta}$  is the gridblock fluid head,  $h_{\beta}^w$  is the wellbore fluid head, and  $T_{\beta}$  is the  
16 transmissivity for the  $\beta$  phase for wellbore-gridblock flow.

17  
18 Peaceman (1978, 1983, 1990) developed formulae for flow between wells and  
19 gridblocks accounting for the large gradients close to the wellbore, and for the effects of  
20 anisotropy in permeability and for gridblock dimensions. These formulae, also used in  
21 Sleep et al. (2000a, 2000b) were more recently used by Lipnikov et al. (2011) for  
22 multiscale simulation of two-phase flow to wells associated in petroleum reservoirs and a  
23 number of other studies (Karimi-Fard and Durlofsky, 2011; Farthing et al., 2012; Preisig  
24 and Prévost, 2012). For a vertical well, the transmissivity for horizontal flow to the well  
25 is given by:

$$26 \quad T_{\beta} = \left[ \frac{2\pi k k_{r\beta} L}{\mu_{\beta}} \right] \left[ \ln \left( \frac{r_0}{r_w} \right) \right]^{-1} \quad (2)$$

27  
28 where  $r_0$  is the well effective radius of influence. Peaceman (1990) showed that  $r_0$  can be  
29 calculated from:

$$r_0 = 0.28 \frac{\left[ \left( \frac{k_y}{k_x} \right)^{1/2} \Delta x^2 + \left( \frac{k_x}{k_y} \right)^{1/2} \Delta y^2 \right]^{1/2}}{\left( \frac{k_x}{k_y} \right)^{1/4} + \left( \frac{k_y}{k_x} \right)^{1/4}} \quad (3)$$

where  $k_x$  and  $k_y$  are permeabilities in the  $x$  and  $y$  directions, respectively, and  $\Delta x$  and  $\Delta y$  are the gridblock dimensions in the  $x$  and  $y$  directions respectively.

Phase relative permeabilities for each wellbore section can be assumed to be the fractions of the length of the wellbore section occupied by the phases of interest. The fractions can be determined from the locations of the interfaces between phases in the well. When a section is completely below the air-water interface but above the water-DNAPL interface, the water phase relative permeability is unity and the air and DNAPL phase relative permeabilities are zero. If the section is completely above the air-water interface the air phase relative permeability is unity and the water and DNAPL phase relative permeabilities are zero. When the section is entirely below the DNAPL-water interface then the DNAPL relative permeability is unity, and the air and water phase relative permeabilities are zero. When a wellbore section contains one or more fluid-fluid interfaces the relative permeabilities are equated to the phase fractions of the wellbore section. In Equation 2 upstream weighting is used for the relative permeability for calculation of wellbore-gridblock flows. The upstream weighting ensures that there will not be flow of any fluid phase from a section of the wellbore into the formation when the saturation of that fluid phase is zero in that section of the wellbore (Sleep et al., 2000).

Wellbore-gridblock flows are calculated for each gridblocks containing a wellbore section by treating the wellbore as another cell in the finite difference grid, with connections to the gridblocks through which it passes. As for regular gridblocks, primary variables are selected from the set of water, gas, and DNAPL phase pressures and saturations, and phase mole fractions. The rules for selection of primary variables is the same as for gridblocks, with the exception that the gas phase pressure is used for all cases where the wellbore contains a nonzero gas phase saturation since when the well is open

1 the gas phase pressure is fixed at atmospheric pressure. If the well is operated as a  
2 vacuum extraction well, the gas phase pressure may be a control variable.

3  
4 Various boundary conditions may be applied to the wells. Fluid levels in the wells may  
5 set simulating skimmer pumps, fluids may be removed at specified rates, or some  
6 combination of specified rate and fluid level, or pressure may be used. Specification of  
7 fluid levels for a well is effectively a specification of fluid saturations in the well as fluid  
8 levels are determined from water saturations and total liquid saturations, Fluid saturations  
9 are set using the sink/source formulation of Forsyth (1988). Wellbore hydraulic heads (or  
10 bottomhole pressures) can also be specified using this sink/source formulation. Pumping  
11 or injection rates are also specified as sinks or sources for the well cell, and various  
12 limiting conditions can also be applied so that fluid levels or hydraulic heads are  
13 controlled between specified limits (for example, see Wu et al., 1996; Wu 2000). As head  
14 drops along the wellbore are not considered, the model is not appropriate for wells in  
15 which high flow rates are imposed such that wellbore frictional losses are significant.

16  
17 The wellbore formulation for DNAPL accumulation presented has been incorporated into  
18 the COMPSIM model described by Sleep et al. (2000a, 2000b), which originated from  
19 the model of Sleep and Sykes (1993a, b) and McClure and Sleep (1996). The model  
20 simulates simultaneous three-phase (gas, water, organic) flow with equilibrium  
21 partitioning of organic compounds between phases (i.e. organic dissolution into the water  
22 phase, organic volatilization into the gas phase, and gas-water partitioning of organic  
23 species according to Henry's Law). Advective-dispersive transport of organic compounds  
24 in the gas and water phase is also simulated. As described in Sleep and Sykes (1993), the  
25 model simultaneously solves the species mass balances for each of the species (water, air  
26 and benzyl alcohol for the present study) in the system.

27  
28 The hysteretic relationships outlined in Parker and Lenhard (1987a) were used for  
29 capillary pressure saturation relationships with organic-water and air-organic capillary  
30 pressures scaled from air-water capillary pressures using Leverett (1941) scaling (scaling  
31 according to ratios of fluid-fluid interfacial tensions, see Parker and Lenhard, 1987a).

1 Entrapped nonwetting fluid saturations (air trapped by water or organic, organic trapped  
2 by water) were functions of fluid saturation histories as described by Parker and Lenhard  
3 (1987a), while relative permeabilities were determined using the expressions given by  
4 Lenhard and Parker (1987b). It should be noted that the Parker and Lenhard (1987a)  
5 relationships do not simulate a discrete entry pressure, unlike the Brooks-Corey  
6 relationships. As the DNAPL pool had reached the extraction well before recirculation  
7 was started, this would not be problematic. In contrast, if the DNAPL pool had not yet  
8 reached the extraction well then accurate simulation of the movement of the front of the  
9 DNAPL pool towards the extraction well would have required the use of a capillary  
10 pressure saturation relationship that had a discrete entry pressure.

11  
12 For the present study, implicit time discretization with upstream weighting of relative  
13 permeabilities and concentrations was used to ensure stable solutions. Nonlinearities in  
14 relative permeabilities and capillary pressures are handled using the Newton-Raphson  
15 method and linearized equations are solved using block incomplete Gaussian elimination  
16 combined with the bi-conjugate gradient stabilized method (see Sleep and Sykes, 1993a  
17 for more detail).

18

### 19 **3. EXPERIMENTAL METHODS**

#### 20 **3.1. Three-Dimensional Pilot Scale Aquifer**

21 The tank (see Figure 2) in which an experiment on DNAPL infiltration, redistribution,  
22 flow to wells, and recovery from wells was conducted is 3.5 m by 3.5 m by 1.7 m high  
23 (Sleep et al., 2000a, 2000b). The walls and bottom of the tank were constructed from 3.2  
24 mm 304 stainless steel sheets. Twenty 5 cm i.d., 1.7 m 1.8 m long Sch 40 aluminum  
25 pipes and five 10 cm i.d. Sch 40 pipes were installed vertically in the tank (not shown in  
26 Figure 2). Various sampling lines and coaxial cables were run through the 5 cm pipes to  
27 different levels in the tank, but were not used for the present study. Five 10 cm i.d. pipes  
28 (W-1, W-12, W-21, and W-25 in Figure 2) served as wells. Each well had five 2.5 cm  
29 wide, 90 cm long, slots cut vertically into their lower halves, starting at 2.5 cm from the  
30 bottom of the tank. The slots were equally spaced radially, and were covered by 100

1 mesh stainless steel screen, to prevent migration of soil fines into the well bores. The tank  
2 also contained a horizontal well, consisting of a 1.2 m long 1.9 cm O.D. aluminum pipe  
3 placed at 70 cm from the bottom of the tank, at the location shown in Figure 2. The  
4 horizontal well was connected to the ground surface by a vertical 1.9 cm O.D. aluminum  
5 pipe connected to the horizontal pipe by an elbow. The horizontal well section had four 3  
6 mm wide equally spaced slots of 1.0 m length and was wrapped in 100 mesh stainless  
7 steel screen.

8  
9 The depth to the water-BA interface was determined with an ohmmeter (Mastercraft)  
10 connected to a pair of wires. The wires, attached to a metal rod, were lowered into the  
11 well until an increase in resistance was observed, indicating that the wires were now in  
12 the BA phase. The air-water interface was measured by lowering a small chain into the  
13 well and observing, with a flashlight, the depth at which the chain encountered the air-  
14 water interface.

### 16 **3.2. Soil Properties**

17 The tank was packed with two types of soil. The finer material, placed at the bottom of  
18 the box to a depth of 83.8 cm was an unscreened soil that was primarily sand, but  
19 contained a fraction of clay-sized particles. The coarser material, placed to a thickness of  
20 86.4 cm on top of the fine sand was a natural sand that was screened. The sands were  
21 placed in the box in lifts of about 10 cm, and compacted with a 30 cm by 30 cm steel  
22 plate. The porosities, measured volumetrically from mineral density and bulk dry volume,  
23 were 0.3 and 0.33 for the coarse sand and the fine sand, respectively. The permeabilities  
24 of the soils, measured using a standard falling head test, were measured to be  $1.23 \times 10^{-11}$   
25  $\text{m}^2$  and  $3.43 \times 10^{-12}$   $\text{m}^2$  for the coarse sand and the fine sand, respectively. The final  
26 values used for the simulation were calibrated slightly to provide a better match to the  
27 data, as discussed below.

28

### 3.3. Benzyl-Alcohol Addition and Fluid level Measurement

Four hundred L of BA (about 5.7% of the tank pore volume) were pumped into the horizontal well (see Figure 2) of the experimental aquifer with a gear pump (Cole-Parmer, Barnant Micropump, drive model #900-574, pump head 184-000). This could represent leakage from a short section of corroded pipe in the subsurface for example. The first 200 L were added over 12.25 hours. The addition of the second 200 L was started 42.25 hours after beginning the first addition and lasted 4.5 hours.

The displacement and distribution of BA were monitored in the months after its introduction in the aquifer. The approximate location of the BA pool was determined by taking level measurements at the five wells.

### 3.4. Benzyl-Alcohol Recovery and Water Recirculation

Around 3280 hours a program of BA recovery was initiated. At the very start of the recovery effort, before starting the recirculation process, slugs of BA were removed from W-12 and W-25 (see Table 1). The water recirculation operation consisted of circulating water from W-12 to W-25. The circulation of the water from W-12 to W-25 created a hydraulic gradient that displaced the pool of BA towards W-12. A constant circulation flow rate of  $563 \text{ mL}\cdot\text{min}^{-1}$ , measured by a rotameter, was used during most of the recovery process (see Table 2). It should be noted that the horizontal well remained in place during the recirculation period. While it is not between W-12 and W-25 there is a possibility that some flow through the horizontal well occurred during the recirculation periods.

After each recirculation period BA that had accumulated at the bottom of W-12 was removed. The volume of benzyl-alcohol pumped quickly from the bottom of W-12 was measured by means of a 2 L flask and then pumped into the waste drum for disposal. The level of BA in W-12 was recorded before and after each slug removal. The removal times and volumes of BA are given in Table 1; the circulation mode times and flow rates are recorded in Table 2. Throughout the duration of the recovery process, water and BA levels were measured in all the observation and recovery wells of the aquifer.

1 Concentrations of BA in the water recirculated from W-12 to W-25 were not measured  
2 and the BA concentration values listed in Table 2 are calibrated model values.

### 3 **3.5. Model parameters, discretization, and boundary conditions**

4 In modeling BA movement in the tank, three-dimensional flow of air, water and BA  
5 phases were simulated. The gas phase was assumed to be a mobile compressible gas,  
6 while water, BA and the soil were considered incompressible. BA was allowed to  
7 dissolve in the water phase and partition to the gas phase. Biodegradation and adsorption  
8 of BA were assumed to be negligible. Properties of BA used in the simulations are given  
9 in Table 3.

10

11 The porosities used in modeling were determined from small-scale experiments with  
12 samples of the soil used in the tank, and were assumed to be representative of the  
13 porosities of the soils in the tank. Sorption was assumed to be negligible. The  
14 permeabilities measured in falling head tests were used as the starting point for  
15 calibration of vertical and horizontal permeabilities of the soils in the tank to provide the  
16 best match to the experimental data (see Table 4), The values are quite close to the falling  
17 head test values, but are lower than those reported in Sleep et al. (2000a, 2000b) that  
18 were determined from slug tests shortly after packing the tank. The tank was not  
19 repacked between studies and lower values for the current study, which are close to the  
20 falling head values, are attributed to compaction of the soil over the three year time  
21 period between the studies. The irreducible water saturation was set to 0.25 consistent  
22 with the results from Sleep et al. (2000b). The maximum residual organic phase  
23 saturations in an organic-water system  $S_{or}^{ow}$ , the maximum residual air phase saturations  
24 in an air-water system  $S_{ar}^{aw}$ , the maximum residual air-organic-water system  $S_{ar}^{aow}$  were  
25 all set to 0.1. These values are lower than the values reported for toluene experiments in  
26 Sleep et al. (2000b), but the properties of BA, particularly the BA water interfacial  
27 tension are quite different than those of toluene (lower organic-water interfacial tension,  
28 greater density, larger viscosity) which may result in different residual nonwetting phase  
29 saturations The van Genuchten air-water capillary-pressure saturation parameters for  
30 imbibition and drainage were taken from Sleep et al (2000b), but the values of  $\alpha$  for

1 drainage and imbibition were calibrated to provide a better match to the well level data,  
2 particularly W-12 data (see Table 4). The air-water  $\alpha$  values are scaled for benzyl alcohol  
3 air and benzyl alcohol water systems using the Leverett scaling factors given in Table 4.  
4 It should be noted that calibration of a number of parameters, as indicated in Table 4,  
5 may result in a non-unique set of parameters. The sensitivity analysis performed helps to  
6 identify the parameters to which the simulations are most sensitive.

7  
8 A finite difference grid with 18, 19 and 30 blocks in the x, y and z directions,  
9 respectively, was used for all the simulations in this study. Gridblocks vertical  
10 dimensions were 5.7 cm, while horizontal gridblock dimensions ranged from 7.5 cm in  
11 blocks containing the wells to 25 cm in gridblocks most distant from the wells. All  
12 boundaries of the model were specified as no flow for all phases, consistent with  
13 conditions in the tank. Gas pressures in the wells were prescribed as atmospheric pressure  
14 as the wells were frequently opened to measure fluids levels. Initial conditions consisted  
15 of hydrostatic equilibrium in both the water and air phases, with the water table initially  
16 1.2 m from the bottom of the tank. BA addition was simulated as a prescribed flux at one  
17 grid block, corresponding to the location of the horizontal well. BA removals from wells  
18 were simulated as specified fluxes for the appropriate well cells, with flux rates  
19 prescribed as averages determined from the total volumes of BA removed (see Table 1)  
20 and the duration of the BA removals (estimated at 2 mins). The fluid circulation from W-  
21 12 to W-25 was simulated as prescribed flow rates for these wells (see Table 2). The  
22 horizontal well was retained in the simulation for the entire simulation including the  
23 recirculation periods. Time steps were dynamically adjusted by the model as a function of  
24 the rate of the convergence of Newton iterations. Time step sizes ranged from as low as  
25 one second when a substantial change was imposed on the system such as BA removal  
26 from a well to 10 - 12 hours when the system was approaching a steady state condition.

27

1 **4. Results and Discussion**

2 **4.1. Experimental Results**

3 Following BA addition, the BA first appeared in W-25 at 136 hours after the start of the  
4 addition (Figure 3a). The BA appeared in W-12 only 450 hours after the first injection  
5 and increased slowly to reach a thickness of 0.8 m, 3300 hours after the first injection.  
6 BA was not detected in W-21 until 2660 hours, and the thickness after 3,280 hours was  
7 approximately 0.1 m. At the end of the infiltration phase, the BA was mostly contained in  
8 the half tank limited by W-21, W-12 and W-25 and no BA DNAPL was detected in W-1  
9 or W-5 at any time during the study. Around 1960 hours the BA level in W-25 dropped  
10 by about 15 cm, but there was no apparent reason for this fairly sudden drop that would  
11 correspond to BA in the well flowing back into the soil in the tank.

12  
13 The first removal of BA from W-12 resulted in a sudden drop in the BA thickness at  
14 3304.8 hours (3a, 3b). Subsequently, the thickness slowly increased (0.08 m in 307.4  
15 hours) until the second removal started at 3612.2 hours, which resulted in a further  
16 decrease of the BA thickness of 0.57 m. The DNAPL level increased again, until the next  
17 removal at 3671.9 hours. This increase was larger than the former increase since the  
18 recirculation process started at 3642.4 hours and accumulated the BA in W-12. Between  
19 3671.88 hours and 4226.9 hours, the succession of removals and water recirculation led  
20 to increases and drops of the BA thickness in W-12. The levels fluctuated between 0.05  
21 m and 0.97 m. Between 4226.8 and 4628.7 hours, the pump was shut down and no  
22 removal was performed. This resulted in a slow thickness increase, from 0.06 m to 0.15  
23 m.

24 **4.2. Model Predictions**

25 Figure 3a compares the BA thicknesses measured and predicted in W-12, W-21, and W-  
26 25, while Figure 3b shows an expanded plot of the measured and predicted W-12 levels  
27 during the BA recovery and water recirculation period. The model predicted that BA  
28 would not reach W-1 and W-5 (results not shown) during the study, consistent with the  
29 experimental observations. During the infiltration and redistribution phase, the  
30 thicknesses are predicted within 0.05 m in W-12. The model predicted a constant BA

1 thickness in W-25 of 0.94 m, while there was a drop in the measured level in W-25  
2 around 1960 hours. The model predicts a constant level before this time that is slightly  
3 lower than the measured value. In the model, once the BA level reaches the top or just  
4 above the top of the screen, water cannot leave the well, and this therefore limits the  
5 further inflow of BA since BA cannot displace water from the well, as all the water is  
6 above the top of the well screen.

7  
8 The model predicts an earlier arrival of DNAPL at W-21 than observed, and also predicts  
9 a greater thickness in W-21 after BA arrival. A sensitivity analysis of model parameters  
10 did not lead to any combination of parameters that could match the measured BA  
11 DNAPL levels in W-21 while still providing a reasonable match to the W-12 and W-25  
12 results. All reasonable combinations of parameters still led to model predictions of earlier  
13 DNAPL arrival at W-21 and higher DNAPL thicknesses at later times than measured. To  
14 limit the extent of model calibration, the possibility that the soil properties in the vicinity  
15 of W-21 were different than the rest of the tank, or that plugging of the W-21 well screen  
16 had occurred was not investigated. The 3-dimensional plot of the DNAPL saturations in  
17 the tank at 3300 hours (Figure 4) shows that the slope of the top of the DNAPL pool is  
18 quite steep in the vicinity of W-21. Thus, a small difference in the actual location of the  
19 wells, particularly the horizontal DNAPL injection well relative to the location of W-21  
20 could produce a substantially different response at W-21.

21  
22 Overall, the model results follow the measured BA thicknesses in W-12 fairly closely  
23 during the water recirculation period. However, in order to achieve this degree of  
24 agreement, it was necessary to adjust the dissolved BA concentration in water  
25 recirculated from W-12 to W-25 during the recirculation period. There is BA DNAPL in  
26 the bottom of W-12 for most of the recirculation period. Since the model is based on the  
27 assumption of equilibrium between the water phase and the DNAPL, the model predicts  
28 that the BA concentration in the water in W-12 is at the solubility limit of 40 g/L.  
29 Applying a flux boundary condition to W-12 for water flow would then remove BA from  
30 W-12 at a rate of 40 g/L times the water pumping rate. However, the water is pumped  
31 from the upper part of the well where the water phase is located, and the water has a

1 limited residence time in the well and is not well mixed with the BA DNAPL.  
2 Consequently, the BA concentration in the water being pumped from the well is less than  
3 the solubility limit. The BA concentration in the water pumped from W-12 to W-25 was  
4 not measured during the study, so model calibration of the BA concentrations in the  
5 water pumped from W-12 was required.

6  
7 The model was modified to allow specification of the BA concentrations in the water  
8 being pumped from W-12 to account for lack of mixing and lack of equilibrium between  
9 the aqueous phase and the BA DNAPL. The manually calibrated extracted aqueous phase  
10 BA concentrations that gave a reasonable visual match between measured and predicted  
11 BA thicknesses in W-12 during BA removal and water recirculation are listed in Table 2.  
12 The calibrated concentration values initially decrease with time and then increase as  
13 pumping of water from W-12 and reinjection into W-25 continues, producing higher BA  
14 concentrations in the water flowing into W-12.

### 15 **4.3. Sensitivity analysis**

16 A sensitivity of the model predictions for benzyl alcohol DNAPL thickness in W-12 and  
17 W-25 was conducted. Sensitivity to intrinsic permeability, BA viscosity, BA density,  
18 hysteresis, irreducible water saturation, residual BA NAPL saturation, and residual gas  
19 saturation were evaluated.

#### 21 **4.3.1 Intrinsic Permeability**

22 The sensitivity to intrinsic permeability of the screened (top) and fine (bottom) sand is  
23 shown in Figures 5a and 5b, respectively. Doubling the top layer permeability results in  
24 an earlier arrival of BA at W-12, while doubling the bottom layer permeability delays the  
25 arrival of BA at W-12. In contrast, halving the top layer permeability delays the BA  
26 arrival at W-12, while halving the bottom layer permeability accelerates the BA arrival at  
27 W-12. The horizontal well used to add the BA is about 15 cm below the interface  
28 between top and bottom sand layers. The permeability sensitivity results indicate that the  
29 first arrival of BA at W-12 is due to flow upwards from the well to the top coarse sand  
30 layer and across this layer to W-12. Decreasing the bottom layer permeability in the

1 model results in the prediction of more BA moving upwards and across the top layer, as  
2 does increasing the top layer permeability. The changes in layer permeabilities have little  
3 effect on the BA arrival time at W-25, as it is very close to the injection well.

4  
5 Increasing the top layer permeability results in an increase in the rate of accumulation of  
6 BA in W-12, while decreasing the top layer permeability has much less effect as at later  
7 times most of the BA is reaching W-12 through the lower layer. This is consistent with  
8 the model predictions of the impact of changing the lower layer permeability where there  
9 is a large impact of changing permeability on the predicted rates of BA accumulation in  
10 W-12. In contrast, the rate of accumulation of BA in W-25 is more sensitive to the top  
11 layer permeability, indicating that the accumulation of BA in W-25 is primarily due to  
12 flow across the top layer.

#### 13 14 **4.3.2 BA Viscosity and Density**

15 The sensitivity of model predictions to viscosity and density are shown in Figures 6a and  
16 6b respectively. Increasing viscosity to  $0.008 \text{ kg m}^{-1} \text{ s}^{-1}$  or decreasing viscosity to  $0.0065$   
17  $\text{kg m}^{-1} \text{ s}^{-1}$  results in faster or slower arrival times, respectively, with similar effects on the  
18 rates of accumulation of BA in W-12 and W-25, respectively. Increasing the BA specific  
19 gravity from 1.05 to 1.098 results in a much more rapid rate of increase in BA level in W-  
20 12, but ultimately lower BA levels in both W-12 and W-25 as the BA spreads out more  
21 along the bottom of the tank.

#### 22 23 **4.3.3 Hysteresis and Capillary Pressure Saturation Parameters**

24 The model predictions for cases with no hysteresis, using either the drainage or  
25 imbibition values of the van Genuchten  $\alpha$  for both layers in the tank are shown in Figure  
26 7a. The results show that the DNAPL arrival, rate of accumulation, and equilibrium  
27 DNAPL thicknesses cannot be accurately predicted in the absence of hysteresis, with  
28 either the drainage or imbibition parameters. Using the drainage  $\alpha$  values results in  
29 earlier arrival and greater DNAPL thickness in W-12 than measured or predicted when  
30 hysteresis is included. Using the drainage  $\alpha$  values increases the capillary pressure  
31 gradients resulting in greater rates of DNAPL flow and earlier arrival of DNAPL at the

1 wells. In addition, increasing  $\alpha$  increases the height of the water-DNAPL interface in  
2 wells for the same water-DNAPL interface in the soil. Analogously, using the imbibition  
3  $\alpha$  values decreases capillary pressure gradients and the difference between DNAPL-water  
4 interfaces in wells and the formation around wells.

5  
6 Increasing or decreasing the van Genuchten  $n$  values by unity individually for the top and  
7 bottom layers (Figure 7b, 7c) has less effect on the rates of DNAPL accumulation in W-  
8 12 and W-25 than neglecting hysteresis. The greatest sensitivity is to the  $n$  value in the  
9 lower sand layer, with a unit decrease in  $n$  producing a greater effect than a unit increase.

10  
11 Adding or subtracting 0.05 to the DNAPL-in-water residual saturation ( $S_{or}^{ow}$ ) for the top  
12 (Figure 7d) and bottom layers (Figure 7e) resulted in small decreases or increases,  
13 respectively, in the arrival time and rate of accumulation of DNAPL in W-12 and W-25.  
14 The greatest impact was produced by the 0.05 increase of  $S_{or}^{ow}$  in the upper soil layer,  
15 due to a greater predicted entrapment of DNAPL in the upper layer. Changes in residual  
16 gas saturations and irreducible water saturations for the upper and lower soil layers had  
17 less effect than changing  $S_{or}^{ow}$  (results not shown)

## 18 **5. Summary and Conclusions**

19 The match between model results and experimental pilot scale data demonstrate the  
20 feasibility of modelling DNAPL accumulation in wells by explicitly simulating fluid  
21 segregation, wellbore fluid storage, and changing water and DNAPL levels in the well.  
22 The sensitivity analysis demonstrated that the model predictions were very sensitive to  
23 the DNAPL viscosity and density, the soil permeabilities, and the imbibition and drainage  
24 parameters of the lower soil layer. Accurate modeling of DNAPL accumulation in wells  
25 requires consideration of hysteresis. In addition, the concentration of benzyl-alcohol in  
26 the water pumped from the extraction well and re-injected into the tank was a crucial  
27 parameter due to the high aqueous phase solubility of BA and limited mixing between  
28 water and DNAPL in the extraction well during water recirculation.

29

1 Given knowledge of soil properties, DNAPL properties, and DNAPL release information  
2 (rate of DNAPL release, duration of release, location of release), it is possible to simulate  
3 the accumulation of DNAPL in wells, and to determine physically feasible rates of  
4 DNAPL removal from the subsurface. It would be possible to determine some soil  
5 property parameters from DNAPL bail tests. However, given the significant number of  
6 soil property parameters required for modeling, independent determination of parameters  
7 would provide a more robust model for forward prediction of DNAPL recovery.

### 9 **Acknowledgments**

10 Financial support from the DuPont Company and the Natural Sciences and Research  
11 Council (NSERC) of Canada is gratefully acknowledged. Input on the pilot scale design  
12 from Calvin Chien of the DuPont Company and Lily Sehayek of the U. S. Army Corps of  
13 Engineers is also gratefully acknowledged.

### 15 **References**

- 16 Alexandra, R., Gerhard, J.I., Kueper, B.H., Hydraulic displacement of dense nonaqueous  
17 phase liquids for source zone stabilization, *Ground Water* 50 (5), pp. 765-774,  
18 2012.
- 19 Behie, A., Collins, D., Forsyth, P.A. and Sammon, P.H., Fully coupled multiblock wells  
20 in oil simulation. *SPEJ*, 25(4), 535-542., 1985.
- 21 Brooks, R.H. and Corey, A.T., Hydraulic properties of porous media. *Hydrol. Pap.* 3,  
22 1964.
- 23 Collins, D., Nghiem, L., Sharma, R. and Li, Y.-K., Field-scale simulation of horizontal  
24 wells. *J. Cdn. Pet. Tech.*, 31(1), 14-21, 1992.
- 25 Farthing, M.W., Fowler, K.R., Fu, X., Davis, A., Miller, C.T., Effects of model resolution  
26 on optimal design of subsurface flow and transport problems, *Advances in Water*  
27 *Resources* 38, 27–37, 2012.

1 Forsyth, P.A., Simulation of nonaqueous phase groundwater contamination. *Adv. Water*  
2 *Resour.*, 11(2), 74-83, 1988.

3 Forsyth, P.A. and Sudicky, E.A., Discrete wellbore simulations of pump-and-treat  
4 strategies for remediation of LNAPL-contaminated aquifers. *J. Cont. Hydrol.*,  
5 31(1), 57-81, 1998.

6 Gerhard, J. I., Kueper, B.H., Hecox, G.R., The influence of waterflood design on the  
7 recovery of mobile DNAPLs, *Ground Water* 36 (2) , pp. 283-29, 1998.

8 Gerhard, J. I., Kueper, B.H., Hecox, G.R. and Schwarz, E. J., Site-specific design for dual  
9 phase recovery and stabilization of pooled DNAPL, *Groundwater Monitoring &*  
10 *Remediation*, 21(2), 71–88, 2001.

11 Karimi-Fard, M., Durlofsky, L.J., An expanded well model for accurate simulation of  
12 well-reservoir interactions, *Society of Petroleum Engineers - SPE Reservoir*  
13 *Simulation Symposium* 1, 688-699, 2011.

14 Lacombe, S., Sudicky, E.A., Frappe, S.K. and Unger, A.J.A., Influence of leaky boreholes  
15 on cross-formational groundwater flow and contaminant transport. *Water Resour.*  
16 *Res.*, 31(8), 1871-1882, 1995.

17 Lenhard, R.J. and Parker, J.C., Measurement and prediction of saturation-pressure  
18 relationships in three-phase porous media systems. *J. Contam. Hydrol.*, 1(4), 407-  
19 424, 1987a.

20 Lenhard, R.J. and Parker, J.C., A model for hysteretic constitutive relations governing  
21 multiphase flow, 2. permeability-saturation relations. *Water Resour. Res.*, 23(12),  
22 2197-2206, 1987b.

1 Lenhard, R.J. and Parker, J.C., Estimation of free hydrocarbon volume from fluid levels  
2 in monitoring wells. *Ground Water*, 28(Jan./Feb), 57-67, 1990.

3 M.C. Leverett, Capillary behaviour in porous solids". *Transactions of the AIME*, 142,  
4 159–172, 1941.

5 Lipnikov, K., Moulton, J.D., Svyatskiy, D., Adaptive strategies in the multilevel  
6 multiscale mimetic (M3) method for two-phase flows in porous media, J.  
7 Multiscale Model. Simul. 9, 991-1016, 2011.

8 McClure, P.D. and Sleep, B.E., Simulation of bioventing for soil and groundwater  
9 remediation. *A.S.C.E. J. Env. Eng.*, 122(11), 1003-1012, 1996

10 Parker, J.C. and Lenhard, R.J., A model for hysteretic constitutive relations governing  
11 multiphase flow, 1, saturation-pressure relations. *Water Resour. Res.*, 23(12),  
12 2187-2196, 1987.

13 Preisig, M., Prévost, J.H., Fully coupled simulation of fluid injection into geomaterials  
14 with focus on nonlinear near-well behavior, *International Journal for Numerical  
15 and Analytical Methods in Geomechanics* 36 (8) , pp. 1023-1040, 2012

16 Peaceman, D.W., Interpretation of well-block pressures in numerical reservoir  
17 simulation. *SPEJ*, 18(3), 183-194, 1978.

18 Peaceman, D.W., Interpretation of Well-Block Pressures in Numerical Reservoir  
19 Simulation with Nonsquare Grid Blocks and Anisotropic Permeability. *SPEJ*,  
20 23(3), 531-543, 1983.

21 Peaceman, D.W., Interpretation of wellblock pressures in numerical reservoir simulation:  
22 part 3 - Off-center and multiple wells within a wellblock. *SPE Res. Eng.*, 5(5),  
23 227-232, 1990.

- 1 Sleep, B.E., Sehayek, L. and Chien, C.C., A modeling and experimental study of light  
2 nonaqueous phase liquid (LNAPL) accumulation in wells and LNAPL recovery  
3 from wells. *Water Resour. Res.*, 36 (12), 3535-3545, 2000a.
- 4 Sleep, B.E., Sehayek, L. and Chien, C.C., Modeling wells in variably saturated soil with  
5 wellbore fluid gravity segregation. *Adv. Water Resour.*, 23(7), 689-697, 2000b.
- 6 Sleep, B.E. and Sykes, J.F., Compositional simulation of groundwater contamination by  
7 organic compounds, 1. model development and verification. *Water Resour. Res.*,  
8 29(6), 1697-1708, 1993a.
- 9 Sleep, B.E. and Sykes, J.F., Compositional simulation of groundwater contamination by  
10 organic compounds. 2. Model applications. *Water Resour. Res.*, 26(9), 1709-1718,  
11 1993b.
- 12 Wu, Y.-S., A virtual node method for handling well bore boundary conditions in  
13 modeling multiphase flow in porous and fractured media. *Water Resour. Res.*,  
14 36(3), 807-814, 2000.
- 15 Wu, Y.S., Forsyth, P.A. and Jiang, H., A consistent approach for applying numerical  
16 boundary conditions for multiphase subsurface flow. *J. Cont. Hydrol.*, 23(3), 157-  
17 184, 1996.
- 18

1	List of Tables
2	Table 1: BA withdrawals from W-12 and W-25
3	Table 2: Data for water circulation from W-12 to W-25
4	Table 3: Properties of BA used in modeling
5	Table 4: Soil properties used in modeling
6	
7	
8	
9	
10	

1

2 **Table 1: BA withdrawals from W-12 and W-25**

<b>Time (hours from first addition)</b>	<b>Recovery from Well 12 (L)</b>	<b>Recovery from Well 25 (L)</b>
3304.60 – 3304.63	0.97	0
3330.2 – 3330.23	0	1.95
3612.2 – 3612.23	4.0	0
3618.2 -3618.23	0	6.05
3671.3 – 3671.33	1.2	0
3741.26 – 3741.29	2.95	0
3762.38 – 3762.41	4.0	0
3771.56 – 3771.59	2.0	0
3814.46 – 3814.49	5.0	0
3888.93 – 3888.96	2.975	0
3908.38 – 3908.41	4.475	0
3931.33 – 3931.36	6.25	0
3955.55 – 3955.58	5.0	0
3979.31 – 3979.34	3.6	0
4003.76 – 4003.79	3.0	0
4051.93 – 4051.96	4.0	0
4125.23 – 4125.26	3.6	0
4219.2 – 4219.23	2.65	0

3

4

1

2 **Table 2: Data for water circulation from W-12 to W-25**

<b>Time (hours from first addition)</b>	<b>Water Flow Rate (mL/min)</b>	<b>BA Concentration (kg/m<sup>3</sup>)</b>	<b>Time (hours from first addition)</b>	<b>Water Flow Rate (mL/min)</b>	<b>BA Concentration (kg/m<sup>3</sup>)</b>
3642.43 – 3644.95	330	28.0	3772.35 – 3787.25	563	21.6
3644.95 – 3647.5	550	28.0	3889.8 – 3908.3	563	21.6
3666.36 – 3670.01	750	28.0	3909.23 – 3931.25	563	21.6
3671.88 – 3689.13	550	26.0	3931.93 – 3955.46	563	24.0
3689.13 – 3689.56	25	26.0	3956.16 – 3979.23	563	26.0
3690.31 – 3691.0	25	26.0	3979.83 – 4003.68	563	26.4
3691.25 – 3695.53	50	24.0	4004.7 – 4051.85	563	28.8
3695.53 – 3720.06	295	24.0	4052.61 – 4125.15	563	30.0
3720.06 – 3741.18	563	24.0	4125.75 – 4219.11	563	31.6
3741.86 – 3762.3	563	21.2	4219.85 – 4226.85	563	38.0
3763.56 – 3771.47	750	21.2			

3

4

1

2 **Table 3: Properties of BA used in modeling**

Property	Value
Molecular Weight	108.14 g mol <sup>-1</sup>
Specific Gravity <sup>a</sup>	1.05
Liquid phase viscosity at 25 C <sup>b</sup>	0.0065 kg m <sup>-1</sup> s <sup>-1</sup>
Aqueous solubility <sup>a</sup>	40.0 kg m <sup>-3</sup>
Water phase diffusion coefficient <sup>c</sup>	1.1574 × 10 <sup>-9</sup> m <sup>2</sup> s <sup>-1</sup>
Gas phase diffusion coefficient <sup>c</sup>	6.944 × 10 <sup>-6</sup> m <sup>2</sup> s <sup>-1</sup>
Vapor pressure at 25°C <sup>a</sup>	20 Pa
BA - air IFT scaling parameter ( $\beta_{ao}$ ) <sup>d</sup>	1.20
BA – water IFT scaling parameter ( $\beta_{ow}$ ) <sup>d</sup>	6.13

3 <sup>a</sup> From JT Baker MSDS

4 <sup>b</sup> from NOAA Cameo Chemicals Database (cameochemicals.noaa.gov)

5 <sup>c</sup> Calculated using correlations in Reid et al. (1987)

6 <sup>d</sup> From Lenhard and Parker (1987a), based on BA-water interfacial tension of  
7 1.175 x 10<sup>-2</sup> N/m.

8

1

2 **Table 4: Soil properties used in modeling**

Property	Screened Sand	Fine Sand
Porosity	0.3	0.33
Van Genuchten $n$	5.0	4.3
van Genuchten $\alpha$ for imbibition <sup>a</sup> , $m^{-1}$	5.3	4.6
van Genuchten $\alpha$ for drainage <sup>a</sup> , $m^{-1}$	3.8	2.66
Irreducible water saturation $S_{wr}$	0.25	0.25
Maximum residual air saturation $S_{ar}^{aw}$ in an air-water system <sup>a</sup>	0.1	0.1
Maximum residual organic saturation $S_{or}^{ow}$ in an organic-water system <sup>a</sup>	0.1	0.1
Maximum residual air saturation $S_{ar}^{aow}$ in an air-organic system <sup>a</sup>	0.1	0.1
Horizontal permeability <sup>a</sup> , $m^2$	$1.5 \times 10^{-11}$	$3 \times 10^{-12}$
Vertical permeability <sup>a</sup> , $m^2$	$7.5 \times 10^{-12}$	$1.5 \times 10^{-12}$

3 <sup>a</sup>Calibrated values.

4

5

6

7

8

9

10

11

12

13

14

15

16

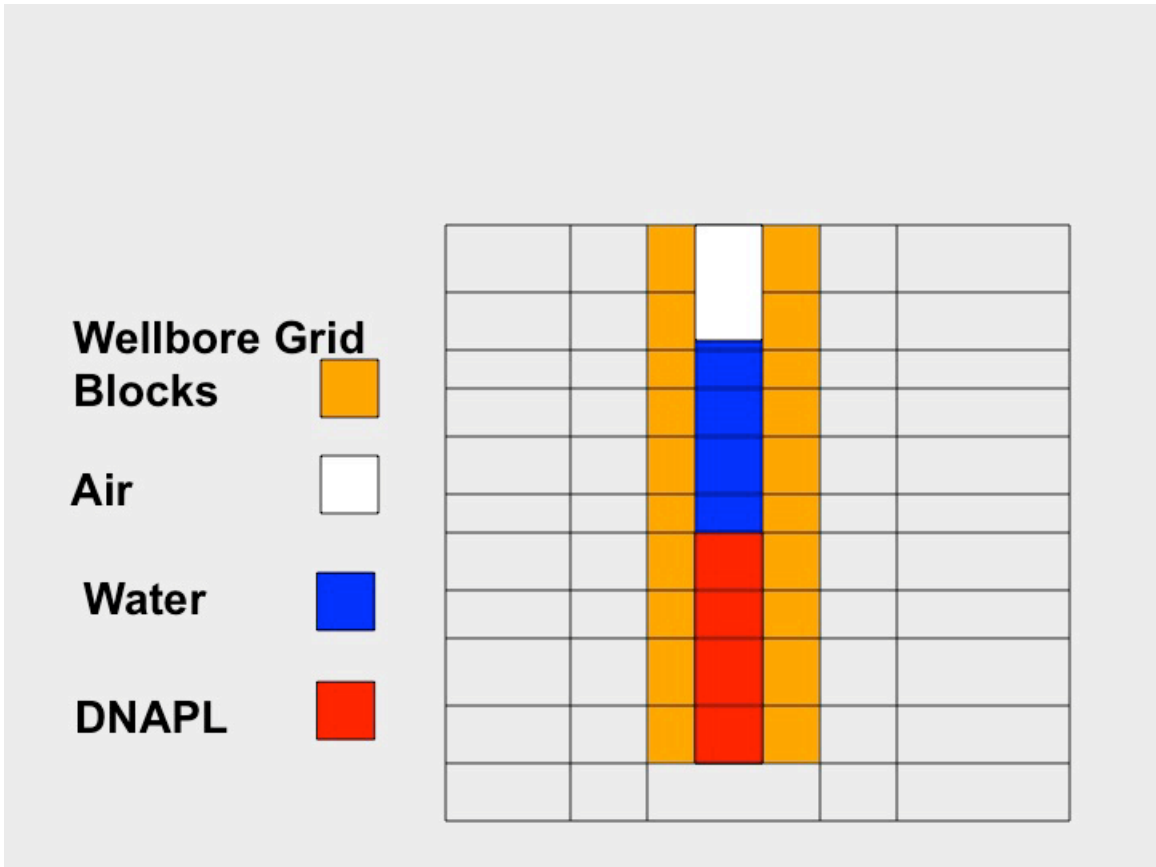


Figure 1: Wellbore configuration

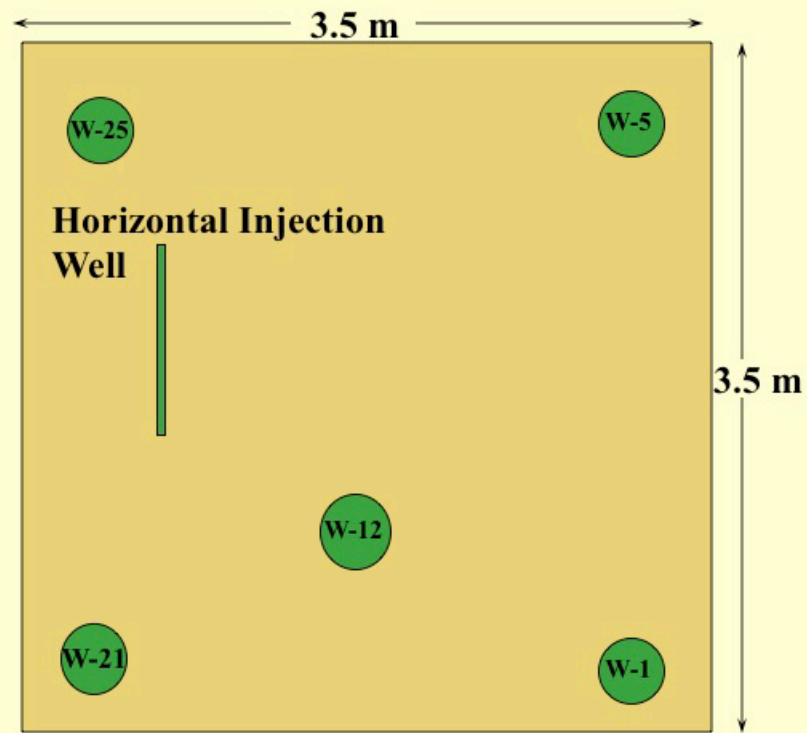


Figure 2: Plan view of tank used for experiments

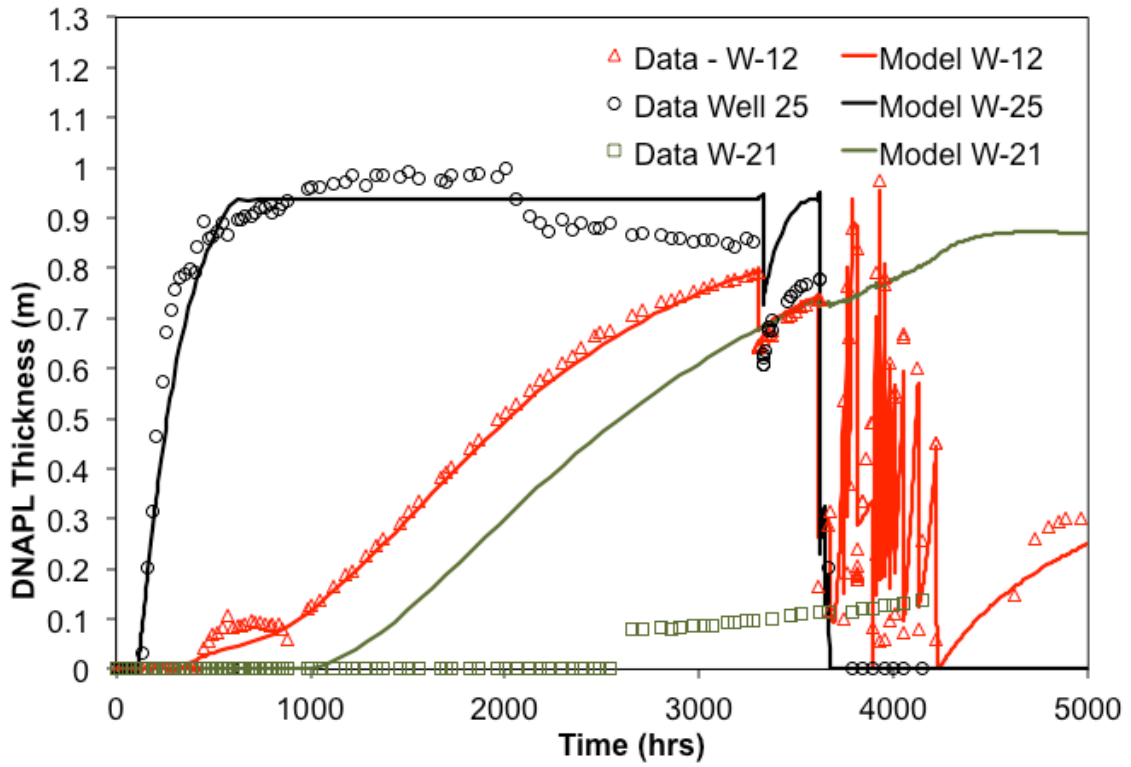


Figure 3a: Measured and predicted DNAPL thicknesses in wells W-12, W-21, and W-25

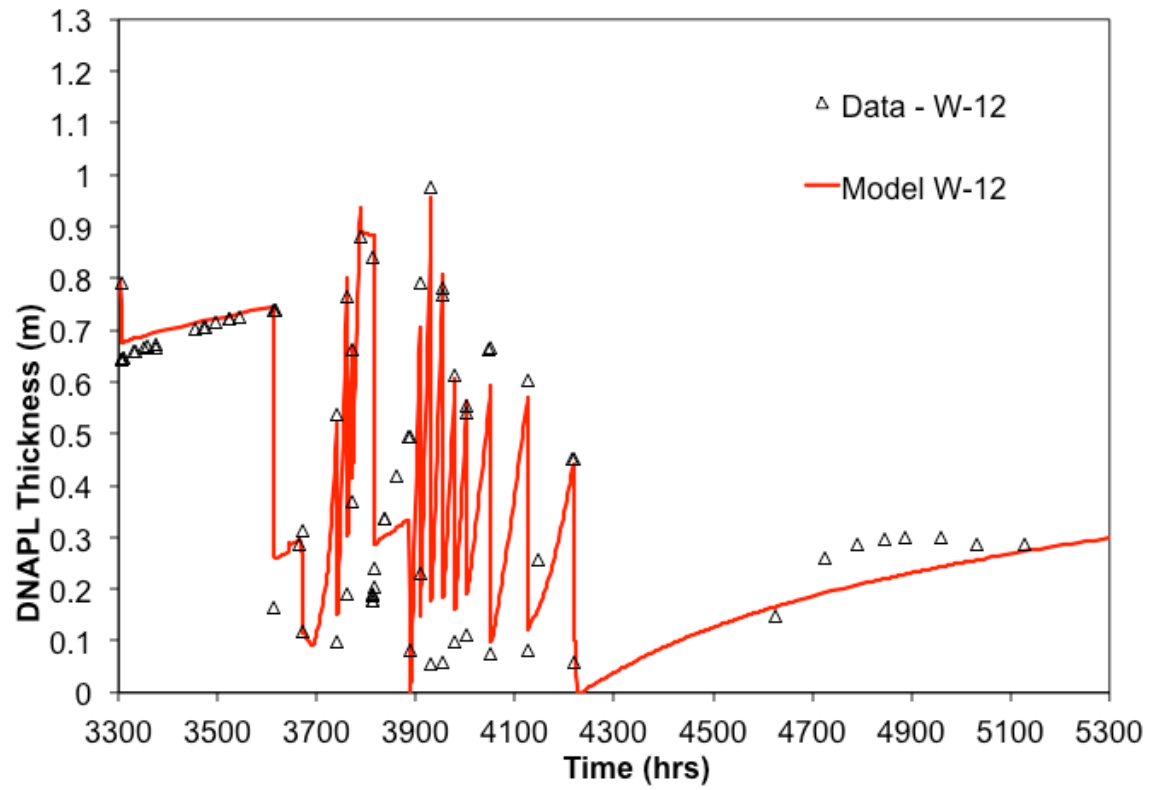


Figure 3b: Measured and predicted DNAPL levels in W-12 during DNAPL recovery period

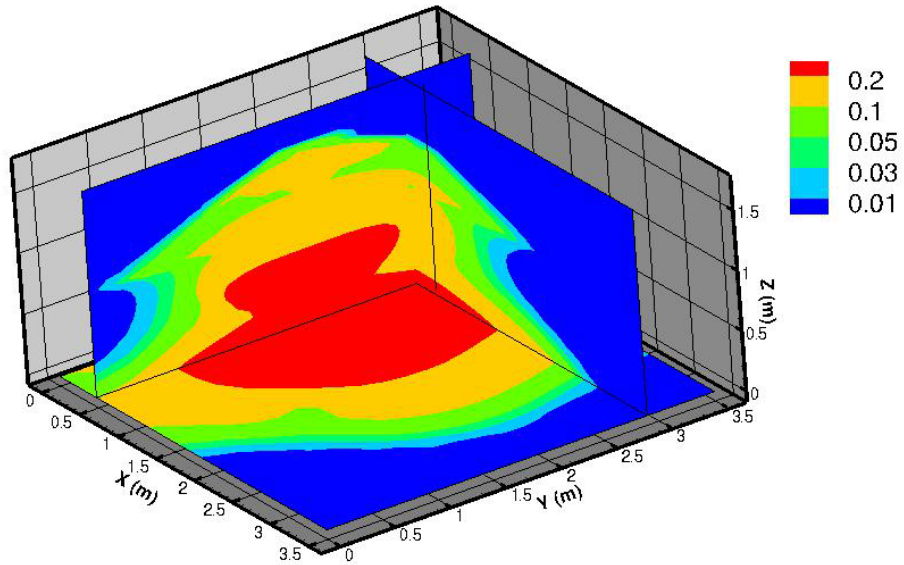


Figure 4: Predicted benzyl alcohol saturations at 3300 hours

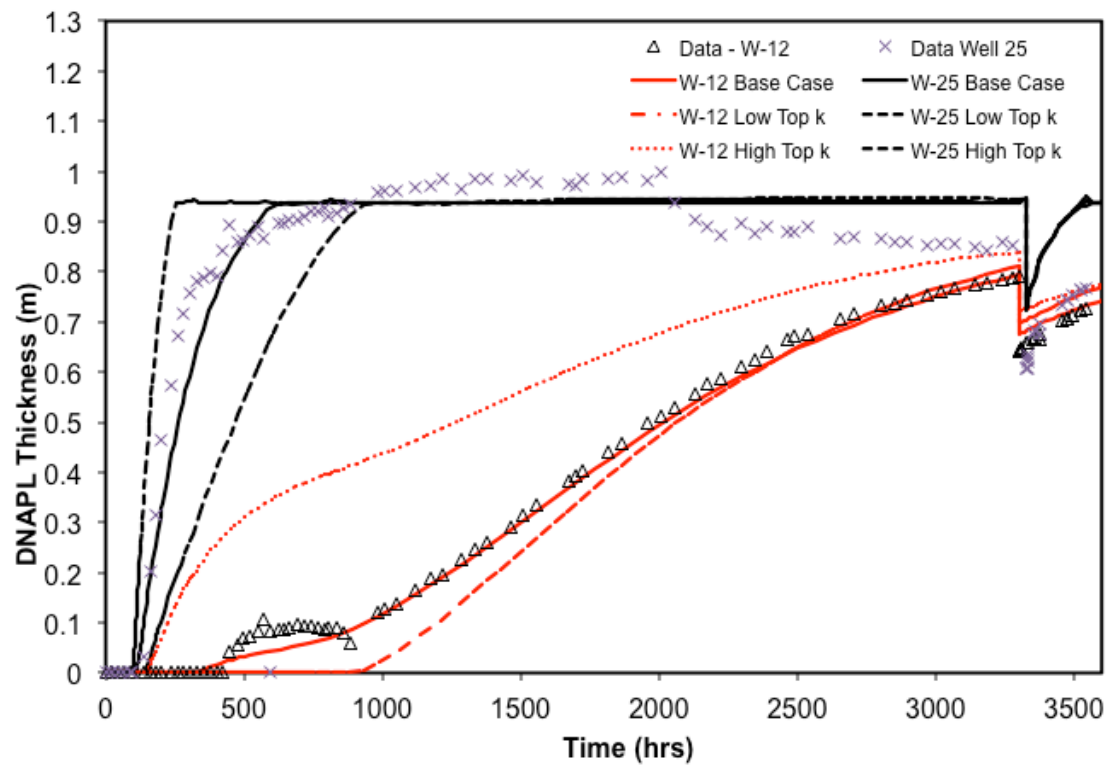


Figure 5a: Sensitivity of predicted DNAPL levels in W-12 and W-25 to permeability of top sand layer in tank

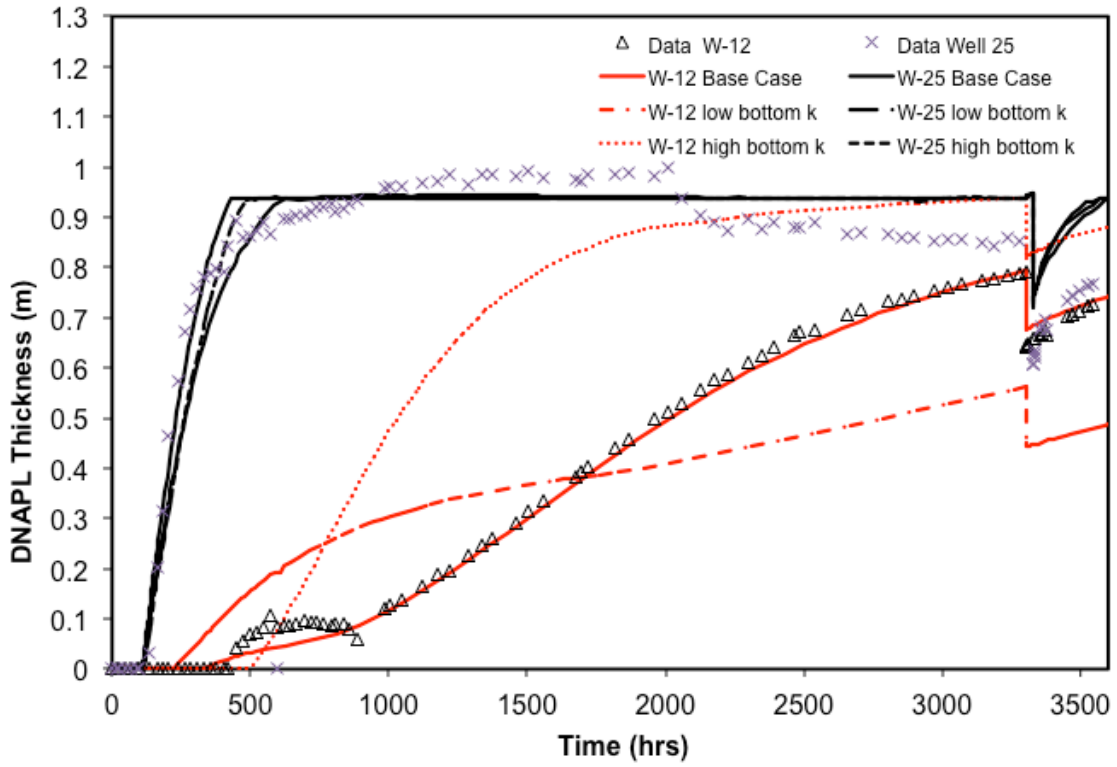


Figure 5b: Sensitivity of predicted DNAPL levels in W-12 and W-25 to permeability of bottom sand layer in tank

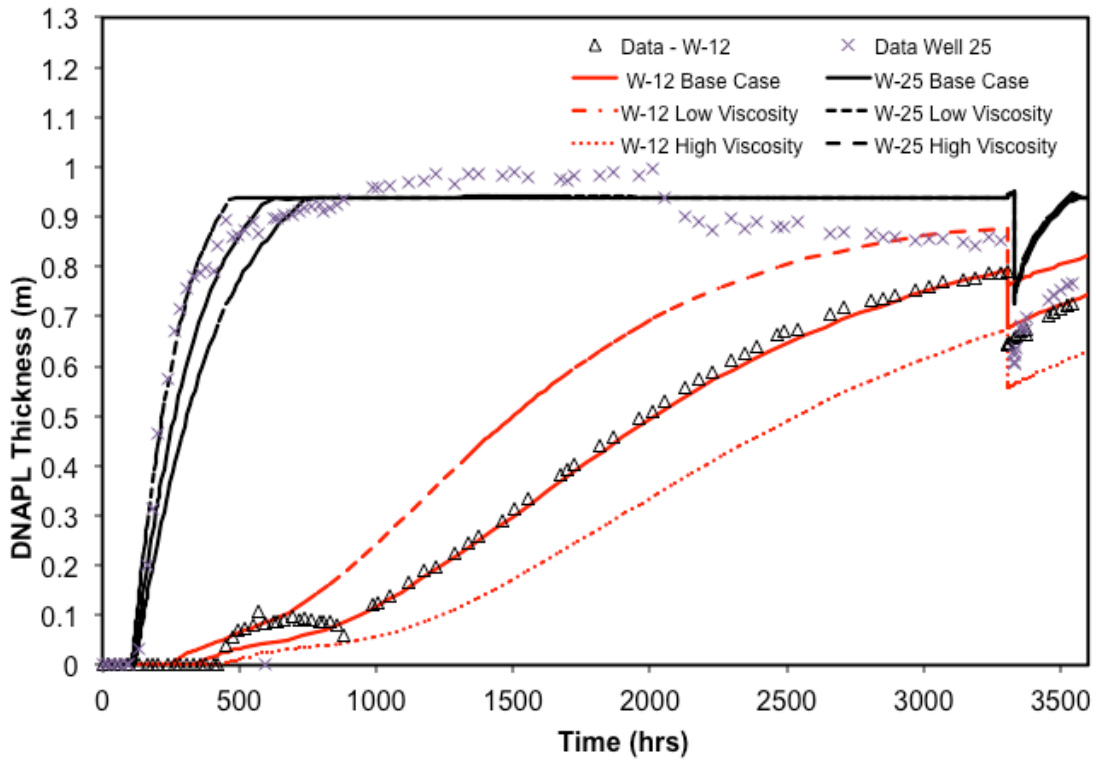


Figure 6a: Sensitivity of predicted DNAPL levels in W-12 and W-25 to BA viscosity

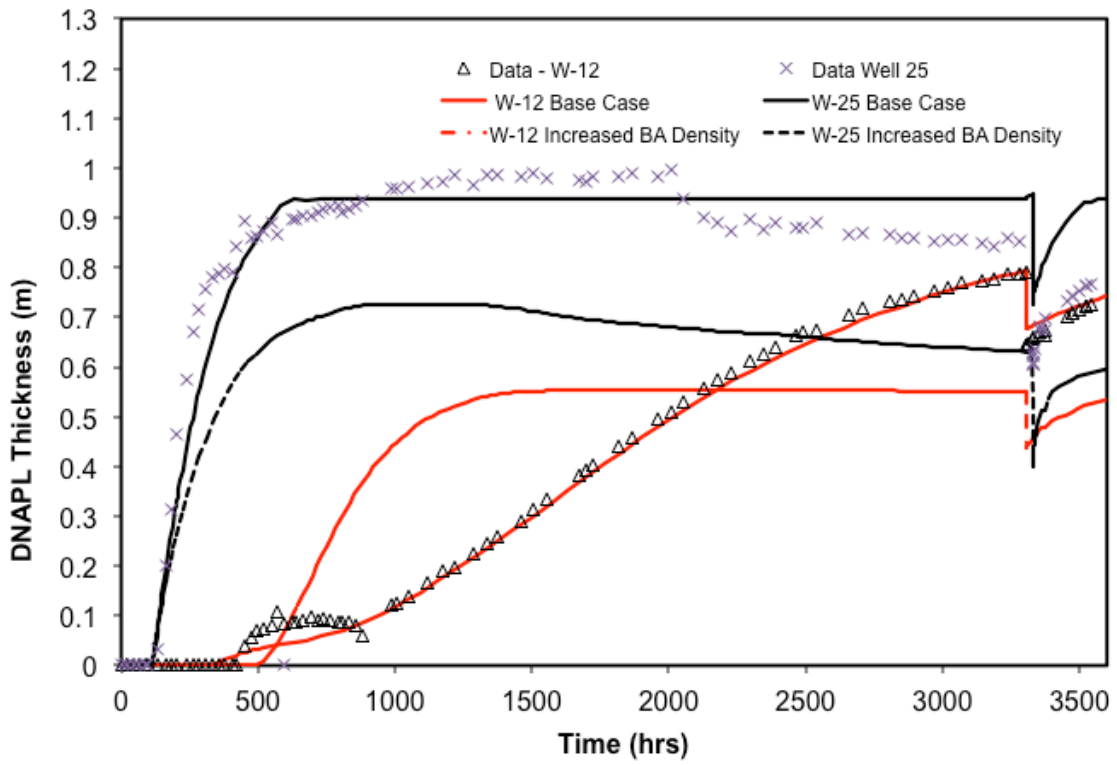


Figure 6b: Sensitivity of predicted DNAPL levels in W-12 and W-25 to BA density

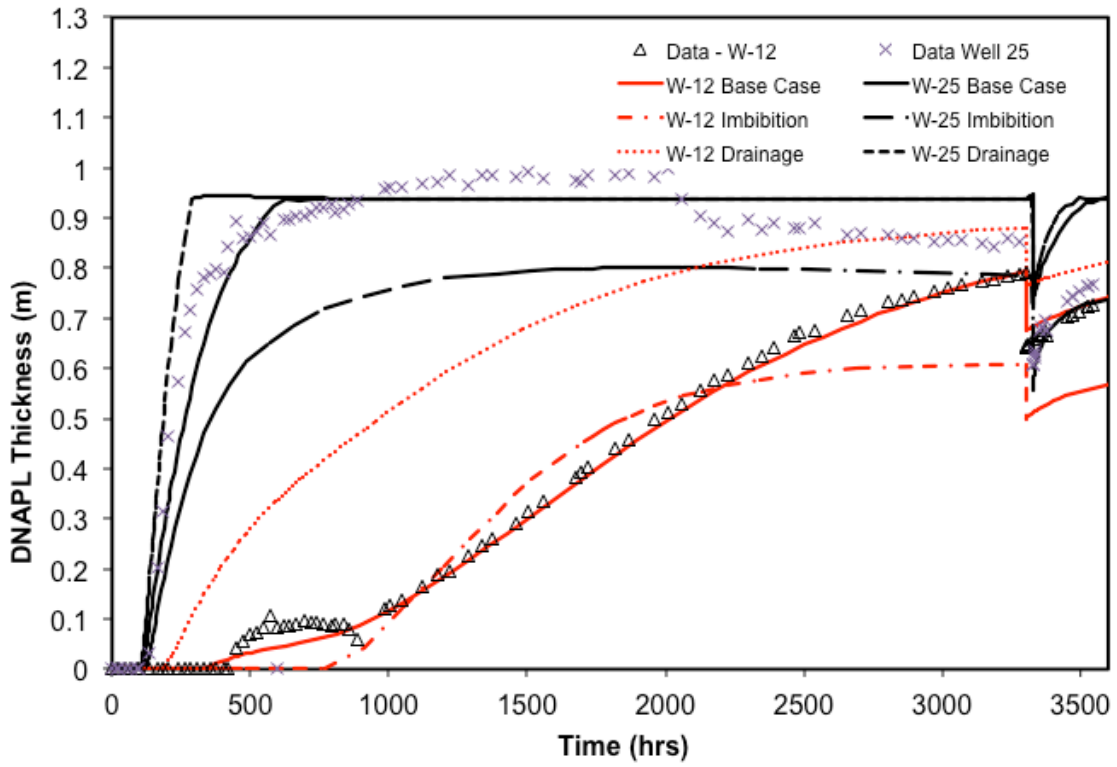


Figure 7a: Sensitivity of predicted DNAPL levels in W-12 and W-25 to van Genuchten parameter  $\alpha$  without hysteresis

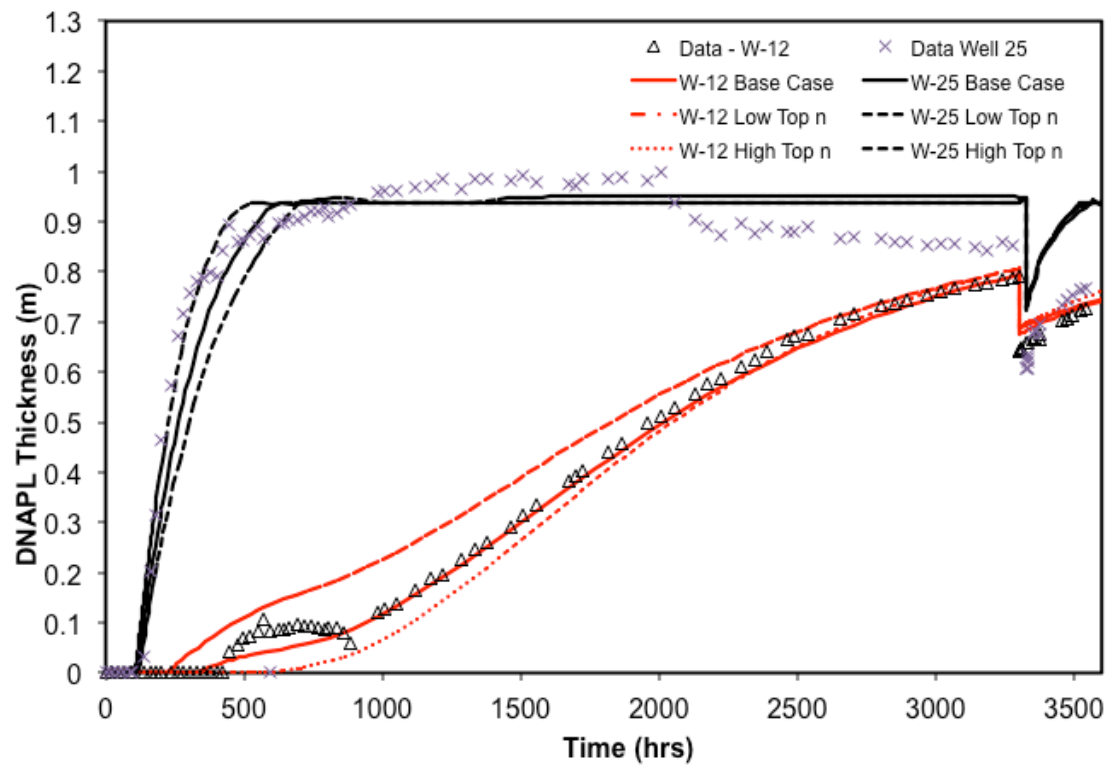


Figure 7b: Sensitivity of predicted DNAPL levels in W-12 and W-25 to van Genuchten parameter  $n$  for top sand layer

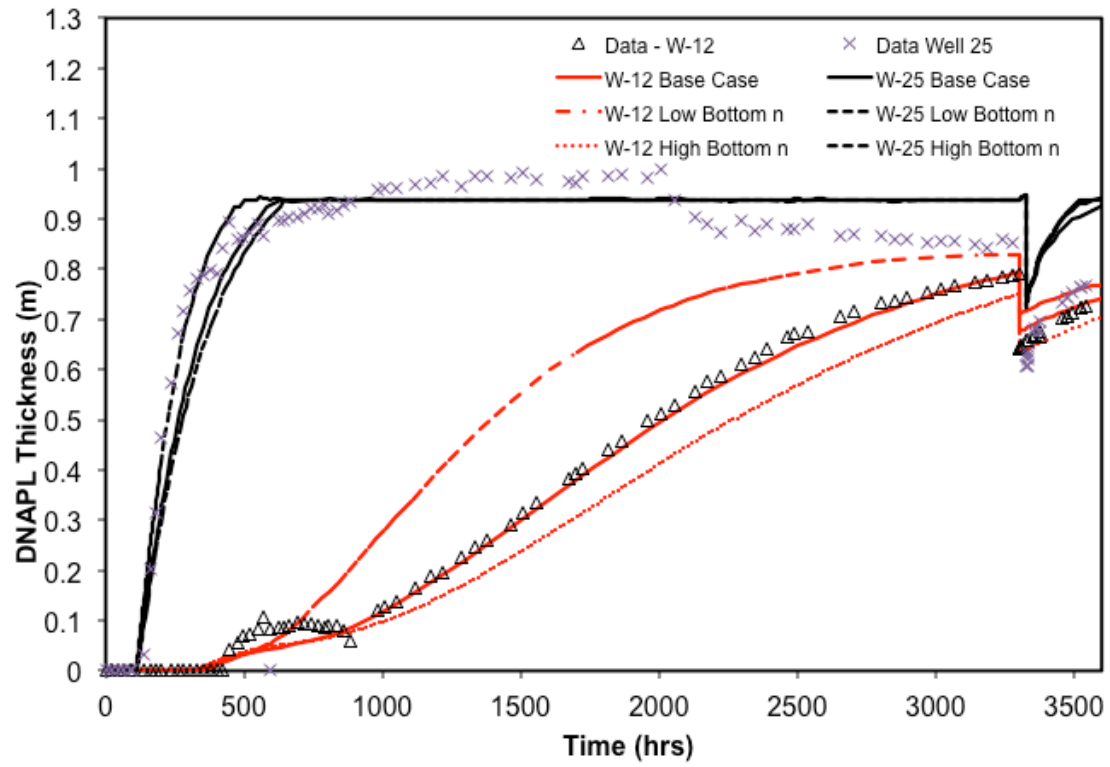


Figure 7c: Sensitivity of predicted DNAPL levels in W-12 and W-25 to van Genuchten parameter n for bottom sand layer

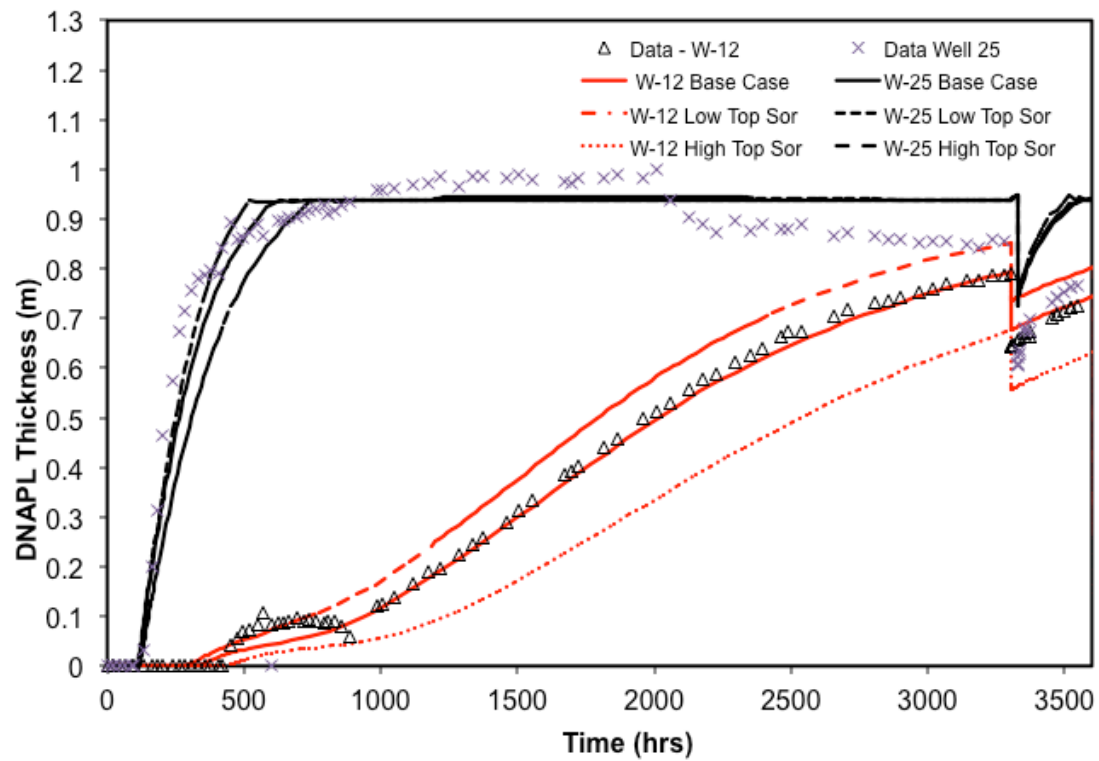


Figure 7d: Sensitivity of predicted DNAPL levels in W-12 and W-25 to residual organic (BA) saturation for top sand layer

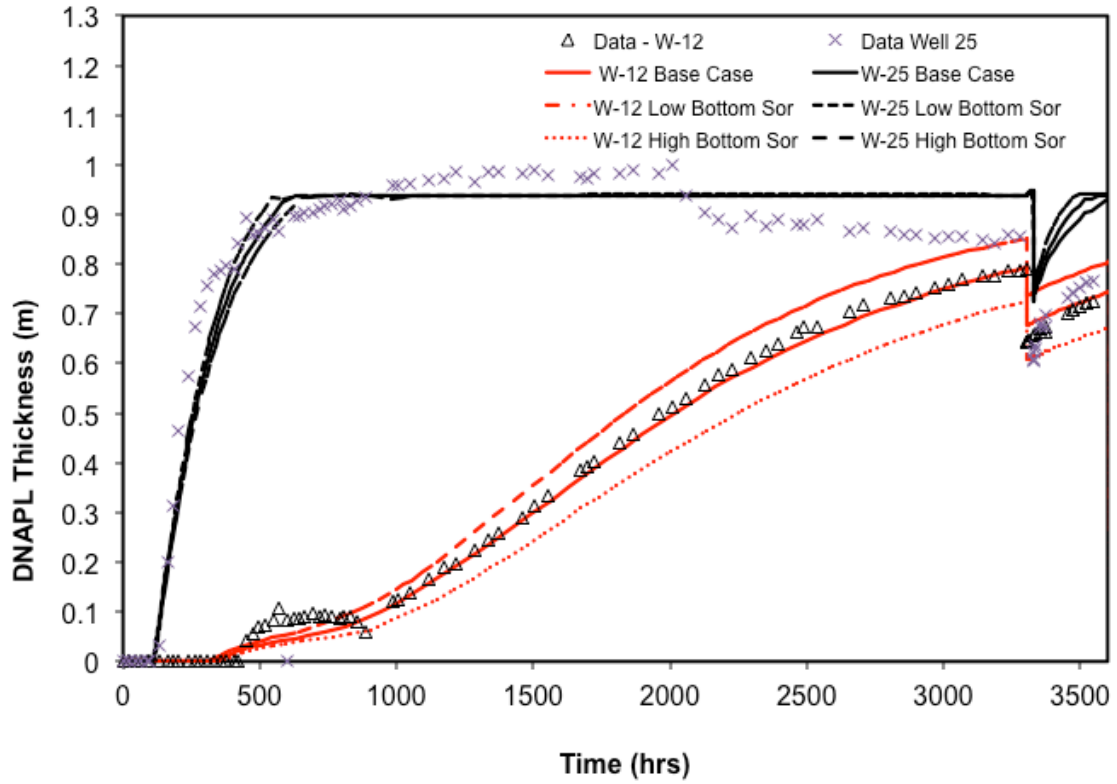


Figure 7e: Sensitivity of predicted DNAPL levels in W-12 and W-25 to residual organic (BA) saturation for bottom sand layer